Dalton Transactions

ROYAL SOCIETY OF CHEMISTRY

PAPER

View Article Online
View Journal | View Issue

Cite this: *Dalton Trans.*, 2024, **53**, 11295

Insight into the inhibitory potential of metal complexes supported by (*E*)-2-morpholino-*N*-(thiophen-2-ylmethylene)ethanamine: synthesis, structural properties, biological evaluation and docking studies†

Saira Nayab, [a,f] Kalsoom Jan,[b,c] Seung-Hyeon Kim,[d] Sa-Hyun Kim,[d] Dilawar Farhan Shams,[e] Younghu Son,[f] Minyoung Yoon *[f] and Hyosun Lee *[f]

Received 6th February 2024,
Accepted 18th May 2024

DOI: 10.1039/d4dt00362d

rsc.li/dalton

A thiophene-derived Schiff base ligand (*E*)-2-morpholino-*N*-(thiophen-2-ylmethylene)ethanamine was used for the synthesis of M(II) complexes, **[TEM(M)X_2]** (M = Co, Cu, Zn; X = Cl; M = Cd, X = Br). Structural characterization of the synthesized complexes revealed distorted tetrahedral geometry around the M(II) center. *In vitro* investigation of the synthesized ligand and its M(II) complexes showed considerable anti-urease and leishmanicidal potential. The synthesized complexes also exhibited a significant inhibitory effect on urease, with IC_{50} values in the range of 3.50–8.05 μM. In addition, the docking results were consistent with the experimental results. A preliminary study of human colorectal cancer (HCT), hepatic cancer (HepG2), and breast cancer (MCF-7) cell lines showed marked anticancer activities of these complexes.

1. Introduction

Schiff bases are versatile and flexible ligands that have gained prominence in bioinorganic chemistry owing to their exceptional chelating abilities allowing the synthesis of structurally diverse complexes.[1–3] The azomethine group in these Schiff bases regulates the activity of metals in various useful catalytic transformations, resulting in various biological, pharmacological, and antitumor effects.[4,5] Schiff base metal complexes have shown a broad scope of biological activities such as antifungal, anti-HIV, antimicrobial, antiviral, and anticancer.[6–11] Metal complexes have tunable coordination environments, oxidation states, and redox potential that can alter the kinetic and thermodynamic properties of these complexes toward biological receptors, in particular, inhibiting enzymatic reactions, enhancing lipophilicity, and altering cell membrane functions.[5,12,13] Therefore, the use of metal complexes as antimicrobial drugs is of considerable interest. In addition, the electron-acceptor and -donor properties of a ligand architecture, the functional groups, and the position of the ligand in a coordination sphere together may govern the properties of metal complexes.[5] The multidrug resistance of several pathogens to the available antibiotics has rapidly increased in the past decades, requiring the development of novel and potent antimicrobial agents with improved pharmacodynamic and pharmacokinetic characteristics.[14,15]

Recently, thiophene-[16–18] and morpholine-derived Schiff base ligands[5,19–21] have become attractive research objects owing to their discovered biological significance. Heterocyclic compounds with nitrogen, sulfur and oxygen donor sites are known for their pharmacological potential, dependent on the type of heterocycle existing in the molecule. A number of mixed ligand complexes possessing O, S, and N-donor binding sites, such as morpholine, thiophene, and furan derivatives,

[a]*Department of Chemistry, Shaheed Benazir Bhutto University, Sheringal Dir (U) 18050, Khyber Pakhtunkhwa, Islamic Republic of Pakistan*
[b]*Department of Plastics Engineering, University of Massachusetts Lowell, Lowell, MA 01851, USA*
[c]*Department of Chemistry, University of Massachusetts Lowell, Lowell, MA 01851, USA*
[d]*BK21 FOUR KNU Creative BioResearch Group, School of Life Science, Kyungpook National University, 80 Daehakro, Bukgu, Daegu, 41566, Republic of Korea*
[e]*Department of Environmental Chemistry, Abdul Wali Khan University Maradan, Khyber Pakhtunkhwa, Islamic Republic of Pakistan*
[f]*Department of Chemistry and Green-Nano Materials Research Center, Kyungpook National University, 80 Daehakro, Bukgu, Daegu, 41566, Republic of Korea. E-mail: myyoon@knu.ac.kr, hyosunlee@knu.ac.kr*

†Electronic supplementary information (ESI) available: ^{1}H NMR, ^{13}C NMR, FTIR, elemental analysis, TGA thermograms, structural refinements, and some biological study results. CCDC 2328624–2328626 for **[TEM(Zn)Cl_2]**, **[TEM(Co)Cl_2]**, and **[TEM(Cd)Br_2]**, respectively. For ESI and crystallographic data in CIF or other electronic format see DOI: https://doi.org/10.1039/d4dt00362d

are completely stable in biological systems owing to their unusual electromagnetic characteristics, eccentric structure, and range of chemical kinetics, which result in their promise for fighting cancer and pathogenic diseases.[22] In this regard, thiophene derivatives have a broad spectrum of biological and pharmacological applications, such as antipsychotic, antianxiety, antifungal, antimicrobial, antioxidant, anticancer, and anti-inflammatory agents. Additionally, most of the marketed drugs including Olanzapine, Sertaconazole, Tioconazol, Tipepidine, Benzocyclidine, Ticlopidine, Clopidogrel, Citizolam, Zileuton, and Tenidap contain a thiophene moiety in their structure.[23] Recently, Co(II) and Cu(II) complexes with *N*′-(3-hydroxybenzoyl)thiophene-2-carbohydrazide have exhibited remarkable cytotoxicity toward MCF-7 and HeLa cell lines in addition to antifungal and antioxidant potential.[24] Similarly, Cu(II), Co(II), Ni(II), and Zn(II) complexes with 2-aminomethylthiophenyl-4-bromosalicylaldehyde showed that the more effective factors for antimicrobial activities are the geometrical shape and the nature of the central atoms; Cu(II) complexes showed superior antibacterial and anticancer properties.[25] Similarly, morpholine is a part of various biologically active complexes and drugs, for instance, Linezolid and Finafloxacin are commercially available antibiotics that possess a morpholine motif.[26] Thus, in our study, we intended to prepare a novel Schiff base ligand system with two different heterocyclic moieties, (*E*)-2-morpholino-*N*-(thiophen-2-ylmethylene)ethanamine (**TEM**) with the aim of obtaining an effective biological agent. The synthesized ligand and its corresponding Co(II), Cu(II), Zn(II), and Cd(II) complexes were screened for antioxidant, anti-urease and anticancer potential. Finally, molecular docking studies were performed to elucidate the mode of action of these complexes and confirm the effective binding of molecules at the active site of the protein.

2. Experimental

2.1. General consideration

The synthesis of the ligand (**TEM**) and its corresponding M(II) complexes was performed by following a bench-top technique. The starting materials, including 2-thiophenecarboxaldehyde (98%), 2-morpholinoethanamine (98%), magnesium sulfate ($MgSO_4$; 99%), cobalt chloride hexahydrate ($CoCl_2{\cdot}6H_2O$; 99%), zinc chloride ($ZnCl_2$; 99%), copper chloride dihydrate ($CuCl_2{\cdot}2H_2O$; 98%), and cadmium bromide tetrahydrate ($CdBr_2{\cdot}4H_2O$; 98%), were obtained from Aldrich. Barium chloride dihydrate ($BaCl_2{\cdot}2H_2O$) and solvents such as methanol (MeOH; 98%), ethanol (EtOH), diethyl ether (Et_2O; 98%), dichloromethane (CH_2Cl_2; 98%), ethyl acetate (EA; 98%), *n*-hexane (*n*-Hex; 98%), and dimethyl sulfoxide (DMSO; 98%) were received from Sigma-Aldrich. NMR solvents such as DMSO-d_6 were obtained from Sigma-Aldrich and stored over 3 Å molecular sieves. 2,2-Diphenyl-1-picrylhydrazyl (DPPH), *Jack bean* (JB) urease, *Bacillus pasteurii* (BP) urease, sodium hypochlorite (NaOCl), urea (CH_4N_2O), thiourea, phenol, and sodium nitroprusside were purchased from Sigma-Aldrich. The *Leishmania* culture was obtained from the microbiology laboratory of the Institute of Pathology and Diagnostic Medicine (IPDM) at Khyber Medical University in Peshawar. Hepatic cancer (HepG2) and breast cancer (MCF-7) cell lines were purchased from Sigma Aldrich, whereas the human colorectal cancer (HCT) cell line was obtained from the Institute of Molecular Biology and Biotechnology (IMBB), University of Lahore, Pakistan.

^{1}H (operating at 500 MHz) and ^{13}C (operating at 125 MHz) NMR spectra of the ligand (Fig. S1 and S2†), and its corresponding Zn(II) and Cd(II) complexes (Fig. S3–S6†) were recorded on a Bruker Avance II 500-NMR spectrometer (Bruker, Billerica, MA) using DMSO-d_6 as a solvent and coupling constants (*J*) are reported in Hertz (Hz). The NMR spectral data were recorded as s = singlet, d = doublet, t = triplet, q = quartet, m = multiplet, and br = broad. The Fourier-transform infrared (FTIR) spectra were recorded on a Bruker FT/IR-Alpha (neat) and the data are reported in cm^{-1} (Fig. S7–S11†). The melting points of M(II) complexes were determined with an IA9100 Electrothermal instrument. The empirical formulas of the synthesized M(II) complexes were determined by elemental analysis (EA) using an EA 1108-elemental analyzer (Carlo Erba, Milan, Italy) (Fig. S12†). Molar conductance in acetonitrile (1×10^{-3} M; Ω^{-1} cm^2 mol^{-1}) solution was determined at room temperature using a digital multimeter 73301 by Yokogawa Meters & Instrument Corperation. Electronic spectra in acetonitrile (1×10^{-4} M) were recorded using a Cary-50 UV–visible spectrophotometer (Fig. 1 and Fig. S13†). Thermogravimetric analysis (TGA) was performed with a heating rate of 10 °C min^{-1} on a thermal analyzer (TGA-Q500) with a mass loss measurement from 25 to 800 °C under an N_2 atmosphere (Fig. S14–S17†).

2.2. Synthesis of the ligand and complexes

2.2.1. Synthesis of (*E*)-2-morpholino-*N*-(thiophen-2-ylmethylene)ethanamine (TEM). CH_2Cl_2 (15.00 mL) solution of 2-morpholinoethanamine (2.00 g, 15.36 mmol) was added dropwise to the solution of 2-thiophene-carboxaldehyde (1.72 g, 15.36 mmol) in CH_2Cl_2 (15.0 mL). The reaction mixture was stirred for 72 h at room temperature. TLC was used to monitor the progress of the reaction using *n*-Hex : EA = 2 : 8 as the developing solvent. After the prescribed time, washing with aqueous NaCl solution was performed. The organic layer was dried over $MgSO_4$ and concentrated. The final product was obtained after vacuum distillation of the crude ligand (2.85 g, 82%). ^{1}H NMR (500 MHz, DMSO-d_6, 298 K): δ = 8.43 (1H, br s, N═C*H*), 7.61 (1H, dt, *J* = 6.64, 3.26 Hz, Ar-*H*), 7.41 (1H, d, *J* = 4.39 Hz, Ar-*H*), 7.10 (1H, dd, *J* = 8.74, 3.70 Hz, Ar-*H*) 3.60 (2H, t, *J* = 6.84 Hz, HC═N(C*H*$_2$-CH$_2$)), 3.52 (4H, t, *J* = 7.0 Hz, (O-(CH)$_2$)), 2.49 (2H, t, *J* = 6.84 Hz, HC═N (C*H*$_2$-CH$_2$)), 2.38 (4H, br s, (N-(CH$_2$)$_2$)). ^{13}C NMR (125 MHz, DMSO-d_6): δ = 155.13 (1C, –N═***C***H–), 142.34 (1C, Ar-***C***), 130.98 (1C, Ar-***C***), 129.23 (1C, Ar-***C***), 127.63 (1C, Ar-***C***), 66.17 (2C, Morpholine-***C***), 58.78 (1C, –N═***C***H$_2$), 57.36 (1C, CH$_2$-***C***H$_2$-N), 53.50 (2C, Morpholine-***C***). FTIR (cm^{-1}): ν(sp^2 C–H) 2944, ν(sp^3 C–H) 2849 ν(C═N) 1631, ν(C═C) 1437, δ(C–H) 1301, ν(C–O)

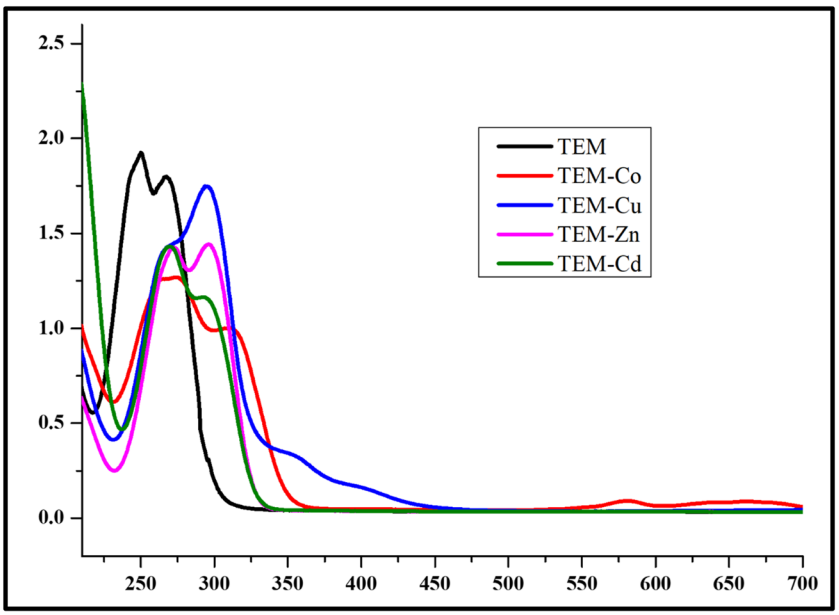

Fig. 1 UV-visible profile of the ligand (**TEM**) and the corresponding **[TEM(M)X_2]** (M = Co, Cu, and Zn; X = Cl; M = Cd, X = Br) complexes.

1142, ν(C–S) 858. UV–vis (acetonitrile; 1×10^{-4} M): 277 (n → π*); 260 (π → π*).

2.2.2. Synthesis of [TEM(Co)Cl_2]. **TEM** (1.00 g, 4.45 mmol) solution in EtOH (10.0 mL) was added dropwise to the $CoCl_2{\cdot}6H_2O$ (1.05 g, 4.45 mmol) solution in EtOH (10.0 mL). The solution was stirred for 2 h and a blue precipitate was formed. The solid was washed with cold EtOH (10.0 mL × 2), followed by washing with Et_2O (5.00 mL × 3). The deep blue final product was obtained after drying *in vacco* at 60 °C (1.51 g, 95%). X-ray quality crystals of **[TEM(Co)Cl_2]** were obtained by the layering of hexane on the CH_2Cl_2 solution of **[TEM(Co)Cl_2]**. M.P. (°C) 152. Analysis of $C_{11}H_{16}Cl_2CoN_2OS$ (%): C 37.30; H 4.55; N 7.91; Found: C 36.99; H 4.60; N 7.74. FTIR (cm^{-1}): $\nu(sp^2$ C–H) 3057, $\nu(sp^3$ C–H) 2910, ν(C=N) 1627, ν(C=C) 1437, δ(C–H) 1301, ν(C–O) 1114, ν(C–S) 858, ν(M–N) 627. UV–vis (acetonitrile; 1×10^{-4} M): 318 (n → π*); 275 (π → π*). Molar conductivity (1.0×10^{-3} M; acetonitrile Ω^{-1} cm^2 mol^{-1}): 14.09.

2.2.3. Synthesis of [TEM(Cu)Cl_2]. **[TEM(Cu)Cl_2]** was synthesized by following a similar procedure to that utilized for **[TEM(Co)Cl_2]** except for utilizing $CuCl_2{\cdot}2H_2O$ (0.75 g, 4.45 mmol) to yield a pale green precipitate (1.30 g, 87%). M.P. (°C) 157. Analysis of $C_{11}H_{16}Cl_2CuN_2OS$: C 36.72; H 4.50; N 7.81; Found: C 36.87; H 4.51; N 7.82. FTIR (cm^{-1}): $\nu(sp^2$ C–H) 3088, $\nu(sp^3$ C–H) 2973, ν(C=N) 1615, ν(C=C) 1454, δ(C–H) 1357, ν(C–O) 1108, ν(C–S) 856, ν(M–N) 580. UV–vis (acetonitrile; 1×10^{-4} M): 305 (n → π*); 268 (π → π*). Molar conductivity (1.0×10^{-3} M; acetonitrile Ω^{-1} cm^2 mol^{-1}): 16.00.

2.2.4. Synthesis of [TEM(Zn)Cl_2]. **[TEM(Zn)Cl_2]** was synthesized by following a similar procedure to that utilized for **[TEM(Co)Cl_2]** except for utilizing $ZnCl_2$ (0.60 g, 4.45 mmol) to yield an ivory precipitate (1.50 g, 93%). X-ray quality crystals of **[TEM(Zn)Cl_2]** were obtained by the layering of hexane on the CH_2Cl_2 solution of **[TEM(Zn)Cl_2]**. M.P. (°C) 168. Analysis of $C_{11}H_{16}Cl_2N_2OSZn$ (%): C 36.64; H 4.47; N 7.77; Found: C 36.56; H 4.45; N 7.82. ^{1}H NMR (500 MHz, DMSO-d_6, 298 K): δ 8.52 (1H, s, N=C*H*), 7.70 (1H, d, J = 3.64 Hz, Ar-*H*), 7.51 (1H, br s, Ar-*H*) 7.15 (1H, dd, J = 8.59 Hz, 3.52 Hz, Ar-*H*), 3.67 (2H, t, J = 6.51 Hz, HC=N(CH_2-CH_2)), 3.59 (4H, t, J = 4.00 Hz, (O-(CH)$_2$)), 2.58 (2H, t, J = 6.40 Hz, HC=N(CH_2-CH_2)), 2.47 (4H, br s, (N-(CH_2)$_2$)). ^{13}C NMR (125 MHz, DMSO-d_6): δ = 184.74 (1C, –N=***C***H–), 130.40 (1C, Ar-***C***), 136.54 (1C, Ar-***C***), 129.44 (1C, Ar-***C***), 128.49 (1C, Ar-***C***), 66.12 (2C, Morpholine-***C***), 65.55 (1C, –N=***C***H_2), 59.28 (1C, CH_2-***C***H_2-N), 54.15 (2C, Morpholine-***C***). FTIR spectra (neat, cm^{-1}): $\nu(sp^2$ C–H) 3058, $\nu(sp^3$ C–H) 2858, ν(C=N) 1637, ν(C=C) 1440, δ(C–H) 1308, ν(C–O) 1058, ν(C–S) 853, ν(M–N) 610. UV–vis (acetonitrile; 1×10^{-3} M): 306 (n → π*); 276 (π → π*). Molar conductivity (1.0×10^{-3} M; acetonitrile Ω^{-1} cm^2 mol^{-1}): 11.15.

2.2.5. Synthesis of [TEM(Cd)Br_2]. **[TEM(Cd)Br_2]** was produced by following a similar process to that described for **[TEM(Co)Cl_2]** except for utilizing $CdBr_2{\cdot}4H_2O$ (1.53 g, 4.45 mmol) and a white precipitate was yielded (2.00 g, 90%). X-ray quality crystals of **[TEM(Cd)Br_2]** were obtained by the layering of hexane on the CH_2Cl_2 solution of **[TEM(Cd)Br_2]**. M. P. (°C) 209. Analysis of elements: $C_{11}H_{18}Br_2CdN_2OS$ (%): C 26.61; H 3.25; N 5.64: Found C 26.88; H 3.33; N 6.04. ^{1}H NMR (500 MHz, DMSO-d_6, 298 K): δ 8.46 (1H, br s, N=C*H*), 7.65 (1H, dt, J = 7.00, 4.98 Hz, Ar-*H*), 7.44 (1H, dd, J = 4.52, 2.36 Hz, Ar-*H*) 7.13 (1H, dd, J = 8.94, 3.49 Hz, Ar-*H*), 3.63 (2H, m, HC=N(CH_2-CH_2)), 3.55 (4H, t, J = 4.57 Hz, (O-(CH)$_2$)), 2.53 (2H, t, J = 7.02 Hz, HC=N(CH_2-CH_2)), 2.42 (4H, br s, (N-(CH_2)$_2$)). ^{13}C NMR (125 MHz, DMSO-d_6): δ = 155.29 (1C, –N=***C***H–), 142.28 (1C, Ar-***C***), 131.14 (1C, Ar-***C***), 129.35 (1C, Ar-***C***), 127.72 (1C, Ar-***C***), 66.16 (2C, Morpholine-***C***), 58.76 (1C, –N=***C***H_2), 57.28 (1C, CH_2-***C***H_2-N), 53.51 (2C, Morpholine-***C***).

FTIR spectra (solid neat cm^{-1}): $\nu(sp^2$ C–H) 3108, $\nu(sp^3$ C–H) 2839, ν(C=N) 1630, ν(C=C) 1435, δ(C–H) 1269, ν(C–O) 1110, ν(C–S) 855, ν(M–N) 611. UV–vis (acetonitrile; 1×10^{-3} M): 294 ($n \rightarrow \pi^*$); 270 ($\pi \rightarrow \pi^*$). Molar conductivity (1.0×10^{-3} M; acetonitrile Ω^{-1} cm^2 mol^{-1}): 18.00.

2.3. X-ray crystallographic data collection and refinement

The data collection for X-ray single crystal structure analysis was performed at room temperature on an XtaLAB mini II diffractometer equipped with a fine-focus Mo Kα X-ray tube (power: 600 W) with a SHINE graphite monochromator (λ = 0.71073 Å) and a hybrid photon counting detector (HyPix-Bantam). The Paratone oil-coated crystals were mounted on a goniometer for the diffraction experiment. The diffraction data were integrated, scaled, and reduced using the Rigaku CrysAlisPro software. The crystal structures were solved using the SHELX structure solution program and refined by full-matrix least-squares calculations with the SHELXL.[27] The positions of all non-hydrogen atoms were refined with anisotropic displacement factors. All hydrogen atoms were placed using a riding model, and their positions were constrained relative to their parent atoms using the appropriate HFIX command in SHELXL-2018/3.[27] The crystallographic data and the results of refinements of **[TEM(Co)Cl$_2$]**, **[TEM(Zn)Cl$_2$]**, and **[TEM(Cd)Br$_2$]** are summarized in Table S1.†

2.4. Biological studies

2.4.1. Antileishmanial assay. The antileishmanial activities of **TEM** and its M(II) complexes, **[TEM(M)X$_2$]**, were determined using previously studied methods.[28] The pre-established culture of *Leishmania major* (*L. major*) was inoculated in 199 medium in Novy–MacNeal–Nicole-medium slants and incubated at 24 °C for 6–7 days. To prepare the stock solution of compounds for the antileishmanial assay, 1.00 mg of each compound was dissolved in 1.00 mL of DMSO to obtain a concentration of 1000 μg mL^{-1}. This stock solution was further serially diluted. Approximately, 180 μL of the 199 medium was added to the wells of 96-well microtiter plates. For each test compound, 20 μL was added to the first well and then serially diluted, maintaining the final volume of 180 μL; 20 μL was discarded from the last well. About 100 μL of the *L. major* suspension was added to each well, with two rows left for positive and negative controls. The DMSO serially diluted in the 199 medium was used as a negative control. Amphotericin B serially diluted in the 199 medium was used as a positive control. Microtiter plates were incubated in a shaker incubator at 24 °C for 72 h. The assay was performed in triplicate. After incubation, 20 μL was taken from each dilution and placed in an improved Neubauer counting chamber to count live parasites under a microscope. The IC_{50} values of compounds exhibiting antileishmanial activity were calculated using the Prism software (GraphPad Software, San Diego, CA).

2.4.2. *In vitro* 2,2-diphenyl-1-picrylhydrazyl free-radical scavenging activity assay. The antioxidant activities of the synthesized ligand and its metal complexes were determined *via* a 2,2-diphenyl-1-picrylhydrazyl (DPPH) free-radical scavenging assay method using a previously reported procedure[29] with a slight modification. First, 0.3 mM DPPH in methanol was prepared. This solution (1.00 mL) was added to 3.00 mL of solutions of **TEM** and its metal complexes in DMSO (10, 20, 30, 40, and 50 μM). The mixture was shaken and incubated in the dark at room temperature for 30 min. Then, the decrease in the absorbance of DPPH was measured at 517 nm (Fig. S18 and S19†). The suppression ratio of DPPH (scavenging activity %) was calculated using eqn (1):

$$\text{Scavenging activity } (\%) = (A_0 - A_1/A_0) \times 100 \quad (1)$$

where A_0 represents the absorbance of DPPH in the absence of an antioxidant and A_1 is the absorbance of DPPH in the presence of an oxidant. All analyses were performed in triplicate, and the IC_{50} was calculated using the percentage of activity. Ascorbic acid was used as a standard.

2.4.3. General procedure of urease inhibitory assay. The urease inhibitory effect of the complexes was measured using the conventional indophenol method with slight modifications.[30] The urease of interest (25 μL), solutions of the studied compounds (5 mL) of various concentrations, and urea (55 μL) were mixed and incubated at 30 °C for 20 min in 96-well plates. A mixture of phenol and nitroprusside (approximately 45 μL, 0.005% w/v) along with a solution of NaOH and NaOCl (0.1% w/v) were added to the above solution. Phosphate buffers were used to maintain the pH at 6.8. The absorption at 630 nm (λ_{max}) was measured using a spectrophotometer (Shimadzu, USA) to determine the urease activity. All assays were performed in triplicate, with thiourea used as a positive control.[31] The percentage inhibition (%) was calculated using eqn (2):

$$\%\text{Inhibition} = 100 - (\text{OD}_{\text{test}}/\text{OD}_{\text{control}}) \times 100 \quad (2)$$

The IC_{50} values for each M(II) complex were calculated using the EZ-fit enzyme kinetics software (Perrella Scientific Inc., Amherst, USA).

2.4.4. Cytotoxicity studies. The cytotoxic potential of the synthesized ligand and its M(II) complexes was assessed on colon and breast carcinoma cells (MCF-7, HepG2, and HCT-116 cell lines) using sulforhodamine B (SRB) as a stain.[32] The cells were injected into a 96-well microtiter plate (10^4 cells per well) after 24 h to allow cell adherence to the plate wall. Before being administered to the cell culture, these test compounds were dissolved in DMSO at a concentration of 1 mg mL^{-1}, and the proper volume of dilution was then applied to the cell culture. These studied compounds and vinblastine were administered to the cells at various concentrations (5, 10, or 20 g L^{-1}). Triplicate wells were made for each dose. The synthesized compounds were cultured with monolayer cells for 48 h at 37 °C in a 5% CO_2 environment. The cells were fixed, washed, and stained with 0.4% (w/v) SRB dissolved in 1% acetic acid for 30 min after 48 h. Tris-EDTA buffer was used to recover the bound stain after four washes in 1% acetic acid and the unbound dye was removed. The optical density in each well was measured at 564 nm using an ELISA microplate reader (United States). The percentage control was calculated

using eqn (3). The results are reported as the IC_{50} (concentration required to inhibit 50% of cell growth) and compared with the vinblastine standard.[32,33]

$$\%\text{Inhibition} = 100 - (OD_{control}/OD_{sample}) \times 100 \quad (3)$$

2.5. Molecular docking protocol

A molecular docking method was used to evaluate the antileishmanial and anti-urease activities of the synthesized Schiff base metal complexes. The three-dimensional (3D) crystal structures of the strains of *Leishmania* (*L. infantum*) and urease (*S. pasteurii*) with the codes 2JK6 and 2UBP were retrieved from the proton data bank. The Molecular Operation Environment (MOE) 2015 software was used for studying molecular docking.[34,35] The charge correction, missing addition of hydrogen, and removal of water molecules from the selected residue were performed before molecular docking. In addition, corrected protonation was achieved using a 3D protonate module in the MOE with a generalized Born/volume integral electrostatic function.[36,37] After molecular docking with an active site, optimal conformation was selected for final docking to conduct docking analysis and calculate the physiochemical descriptors.[38]

3. Results and discussion

3.1 Synthesis and physical characterization

As per the synthetic protocols presented in Scheme 1, a single-step condensation reaction of thiophene-2-carboxaldehyde with 2-morpholinoethanamine yielded **TEM** as light yellow oil. Thin-layer chromatography was used to assess the progress and completion of the reaction (developing solvent *n*-Hex : EA = 9 : 1; R_f = 0.56); the formation of the ligand was verified by the disappearance of aldehyde spots. Further confirmation was obtained from the FTIR spectrum, where the band of ν(C=O) disappeared and a new ν(C=N) band appeared.[38,39] The synthesized **TEM** was further purified *via* vacuum distillation.

The M(II) complexes of **TEM** ([**TEM(M)X$_2$**], M = Co, Cu, Zn; X = Cl; M = Cd, X = Br) were obtained in high yields (87–93%) *via* the direct ligation of **TEM** with M(II) salts at appropriate molar ratios in anhydrous EtOH at 25 °C. The M(II) complexes were stable and soluble in acetonitrile, CH_2Cl_2, $DMSO_4$, dimethylformamide, and tetrahydrofuran at ambient temperature. However, in aqueous media, the ligand was found to be practically insoluble, whereas the complexes showed improved solubility compared to the ligand. The structural characterization of **TEM** and its M(II) complexes, **[TEM(M)X$_2$]**, was performed *via* ^{1}H, ^{13}C NMR, FTIR, and elemental analyses. In the ^{1}H NMR spectra, the characteristic signal of the imine proton of the ligand appeared at 8.43 ppm and shifted to a high ppm in the corresponding Zn(II) and Cd(II) complexes.[14] In addition, the shift in the signals of the imine carbons in the ^{13}C NMR of the complexes further confirmed their structures.

The characteristic ν(C=N) imine peak was observed at 1637 cm^{-1} in the FTIR spectrum of free **TEM** (Fig. S9†).[38–41] This vibration mode slightly shifted to a low frequency (1616 cm^{-1}) in the spectra of the corresponding M(II) complexes, signifying that complexation occurred by the bonding of imine nitrogen with the M(II) center.[40,41] The C=N bond became weak upon chelation owing to the inductive effect of a lone electron pair on imine nitrogen shared with the M(II) center.[41] The medium-to-weak bands in the 2900–3100 cm^{-1} region of the **TEM** spectrum were assigned to aliphatic and aromatic ν(C–H) stretching vibrations.[40,41] The chelation of metal ions through the nitrogen of **TEM** was also confirmed by the presence of new bands at 580–627 cm^{-1} in the spectra of M(II) complexes, which were assigned to ν(M–N) (Fig. S9–S13†).[14,40,41] The peak in the 1454–1437 cm^{-1} region was assigned to symmetrical and asymmetrical ν(C=C) stretching vibrations of the thiophene ring.[42] Herein, the (C–S) stretching vibrations in **TEM** were observed as a peak at 867 cm^{-1}, which red shifted upon complexation.[43] Notably, the band of ν(M–S) stretching vibrations was not observed at 450–430 cm^{-1} in the spectra of complexes, confirming that the sulfur in thiophene did not participate in complexation.[14,44,45] The characteristic ν(C–O) band in the FTIR spectra of the ligand and its M(II) complexes appeared in the 1100–1150 cm^{-1} range.[46] In addition, contents of C, H, and N obtained through elemental analysis of the synthesized M(II) complexes agreed with the

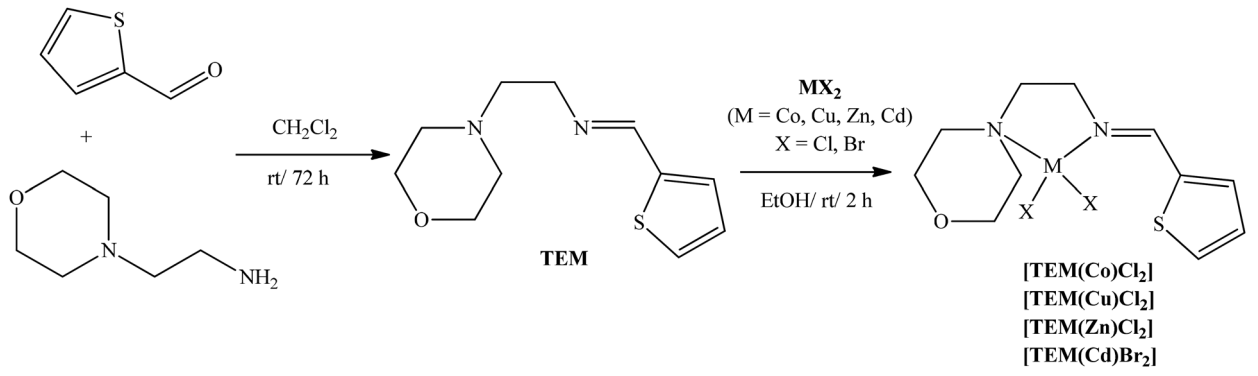

Scheme 1 Scheme illustrating the synthesis of **TEM** and its corresponding M(II) complexes.

proposed structures. The molar conductance of the synthesized complexes was determined at ambient temperature using freshly prepared solutions of the complexes in acetonitrile (1×10^{-3} M). The low conductance values indicated the non-electrolytic nature of the synthesized complexes.[47] The conductivity values of the synthesized complexes remained unchanged even after 5 h, demonstrating the stability of the studied complexes in solution. Additionally, the lower values of molar conductance signify a 1 : 1 ratio for the synthesized complexes in the solution phase. The UV–vis spectra of **TEM** and **[TEM(M)X_2]** (M = Co, Cu, and Zn; X = Cl; M = Cd, X = Br) complexes were recorded in acetonitrile (Fig. 1). Absorption bands at approximately 239–270 nm were ascribed to the $\pi \rightarrow \pi^*$ transitions of the aromatic ring.[48] Bands corresponding to the $n \rightarrow \pi^*$ electronic transition owing to the imine C=N group were observed at approximately 275–355 nm.[14,35] A bathochromic shift was observed in the absorption wavelength of complexes, indicating that a lone pair of electrons of N is donated to M(II) ions upon complexation (Fig. 1).[35,48] In addition, representative time–stability curves of **[TEM(Cd)Br_2]** at 0 and 72 h are shown in Fig. S13.† No considerable changes are observed in the intensity or position of the absorption pattern of the studied complexes during this period, confirming the stability of the complexes in solution. In addition to the $\pi \rightarrow \pi^*$ and $n \rightarrow \pi^*$ transitions, **[TEM(Co)Cl_2]** also exhibited peaks at 575 nm, assigned to $^4A_2 \rightarrow {}^4T_1$ (F), and at 664 nm, assigned to $^4A_2 \rightarrow {}^4T_1$ (P).[49] In case of **[TEM(Cu)Cl_2]**, weak bands appeared at 358 ($^1A_1g \rightarrow {}^1B_1g$) and 394 ($^2B_1g \rightarrow {}^1A_1g$) nm and were attributed to the ligand-to-metal charge transfer (LMCT) transitions, suggesting square planner geometry.

The thermal stability profile of **[TEM(Co)Cl_2]** is presented in Fig. S14.† The TGA curve of **[TEM(Co)Cl_2]** shows no weight loss up to 235 °C, thereby inferring the absence of coordinated water molecules (Fig. S14†). A single-step decomposition observed at 240–450 °C was attributed to the decomposition of the ligand, with a weight loss of 54%. In the case of the Cu(II) complex, **[TEM(Cu)Cl_2]**, no weight loss is observed up to 230 °C. The loss between 250 °C and 370 °C, with an exothermic peak in the 250–350 °C range was associated with the loss of chloride ions and the thiophene moiety. A second decomposition begins at 460 °C and ends at 640 °C, resulting in a horizontal thermal curve above 670 °C (Fig. S15†).[50] The **[TEM(Zn)Cl_2]** profile is stable up to 210 °C. The single-step decomposition starts at 215 °C and ends at 450 °C, exhibiting an exothermic peak at 250–310 °C, associated with the loss of bromide ions and the thiophene moiety. The second stage of degradation at 500–700 °C with a weight loss of 35% indicates the decomposition of **[TEM(Zn)Cl_2]** (Fig. S16†).

The TGA profile of **[TEM(Cd)Br_2]** shows a two-step decomposition. The decomposition starts with an exothermic peak at 200–320 °C, attributed to the loss of bromide ions and dissociation of the thiophene moiety, resulting in a weight loss of 39%. The residue undergoes a second stage of degradation at 460–610 °C, which was attributed to the decomposition of the ligand, resulting in a weight loss of 48%. The thermal curve is horizontal above 620 °C (Fig. S17†).

3.2. Molecular structure

The single-crystal X-ray diffraction studies were performed to determine the geometries of the Co(II) complexes. The ORTEP diagrams of **[TEM(M)X_2]** (M = Co, Zn; X = Cl; M = Cd, X = Br) are shown in Fig. 2–4, and the selected bond lengths and angles are listed in Table 1.

The coordination environment around the M(II) center in **[TEM(M)X_2]** (M = Co, Zn; X = Cl; M = Cd, X = Br) is distorted tetrahedral, obtained *via* coordination to the *N*,*N*-bidentate

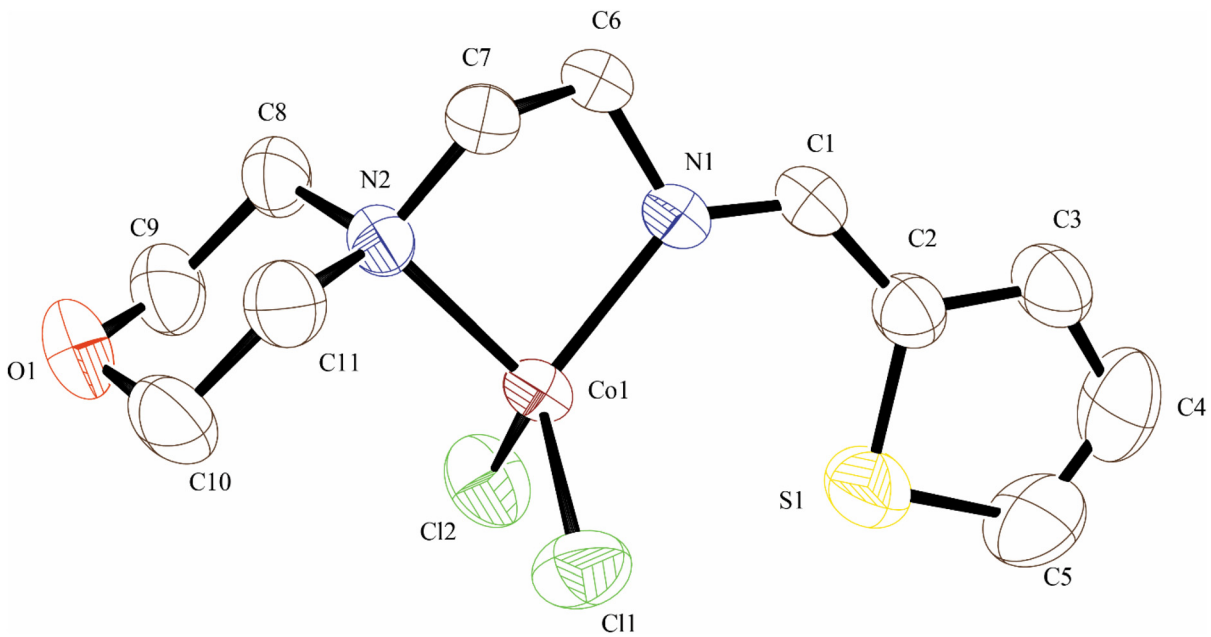

Fig. 2 Molecular structure of [TEM(Co)Cl_2] with thermal ellipsoids at 50% probability.

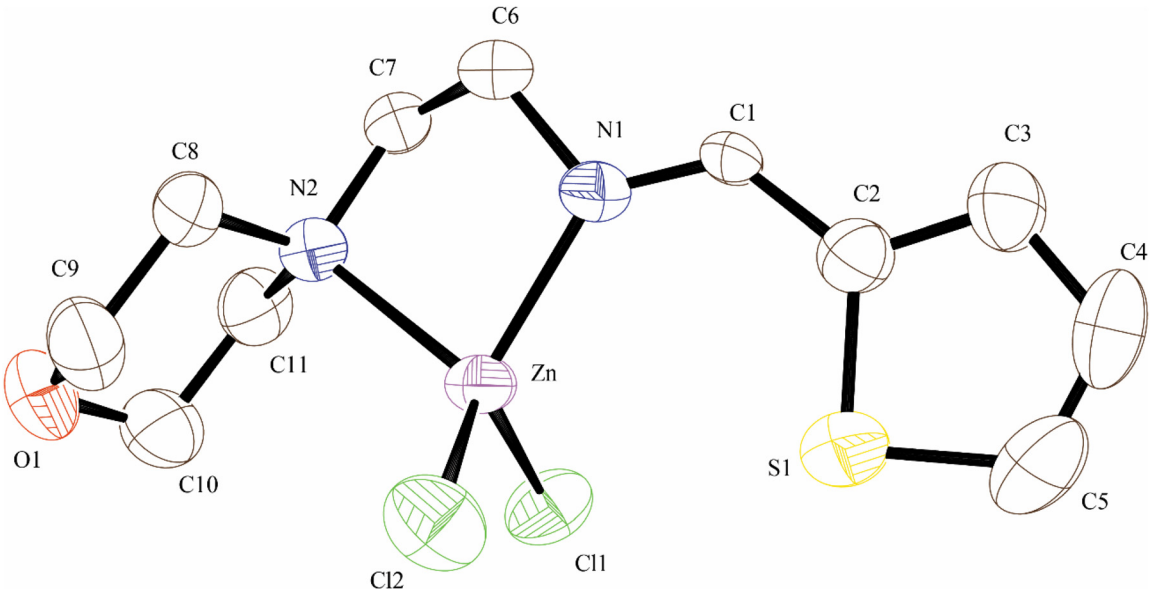

Fig. 3 Molecular structure of **[TEM(Zn)Cl_2]** with thermal ellipsoids at 60% probability.

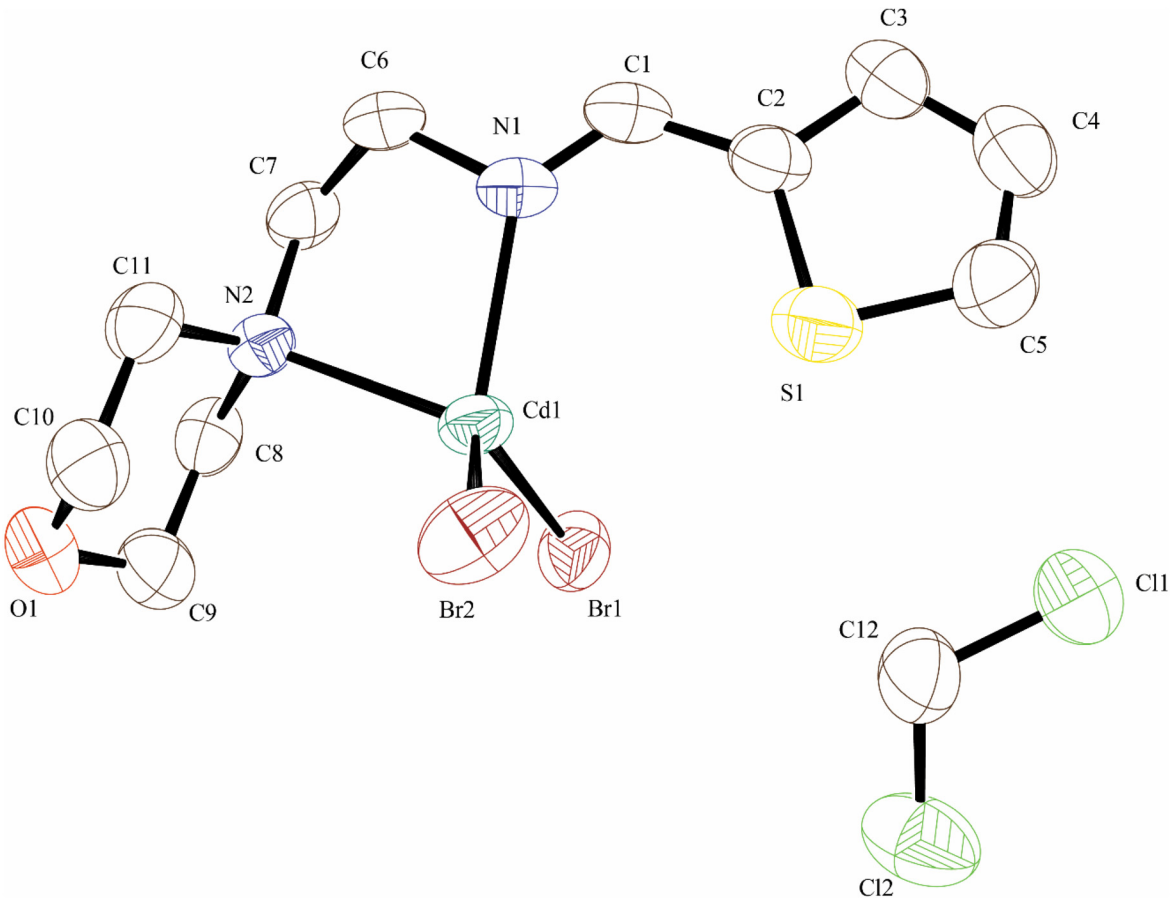

Fig. 4 Molecular structure of **[TEM(Cd)Br_2]·CH_2Cl_2** with thermal ellipsoids at 60% probability.

ligand, along with two halide ligands. The τ_4 value was used as a simple metric for quantitative evaluation of geometry of four-coordinated complexes (Table 2).[51] Complexes with an ideal square planar geometry are characterized by τ_4 of 0; at the same time, τ_4 is equal to 1 in the case of ideal tetrahedral geometry. The τ_4 values of the studied complexes were com-

Table 1 Selected bond lengths (Å) and angles (°) of **[TEM(Co)Cl$_2$]**, **[TEM(Zn)Cl$_2$]**, and **[TEM(Cd)Cl$_2$]**

[TEM(Co)Cl$_2$]		**[TEM(Zn)Cl$_2$]**		**[TEM(Cd)Cl$_2$]**	
Bond lengths (Å)					
Co(1)–N(1)	2.035(2)	Zn(1)–N(1)	2.060(2)	Cd(01)–N(1)	2.342(3)
Co(1)–N(2)	2.130(2)	Zn(1)–N(2)	2.152(3)	Cd(01)–N(2)	2.294(3)
Co(1)–Cl(1)	2.2213(8)	Zn(1)–Cl(1)	2.2154(9)	Cd(01)–Br(1)	2.5305(5)
Co(1)–Cl(2)	2.2258(7)	Zn(1)–Cl(2)	2.2164(9)	Cd(01)–Br(2)	2.5092(5)
N(1)–C(1)	1.280(3)	N(1)–C(1)	1.274(4)	N(1)–C(1)	1.280(6)
N(1)–C(6)	1.477(3)	N(1)–C(6)	1.482(4)	N(1)–C(6)	1.478(6)
Bond angles (°)					
N(1)–Co(1)–N(2)	85.90(8)	N(1)–Zn(1)–N(2)	85.66(10)	N(1)–Cd(1)–N(2)	79.27(13)
N(1)–Co(1)–Cl(1)	116.19(6)	N(1)–Zn(1)–Cl(1)	115.75(8)	N(1)–Cd(1)–Br(1)	105.47(9)
N(2)–Co(1)–Cl(1)	104.53(6)	N(2)–Zn(1)–Cl(1)	104.65(7)	N(2)–Cd(1)–Br(1)	113.03(10)
N(1)–Co(1)–Cl(2)	115.40(7)	N(1)–Zn(1)–Cl(2)	114.10(8)	N(1)–Cd(1)–Br(2)	114.55(9)
N(2)–Co(1)–Cl(2)	118.77(6)	N(2)–Zn(1)–Cl(2)	118.52(7)	N(2)Ta–Cd(1)–Br(2)	115.36(9)
Cl(1)–Co(1)–Cl(2)	112.52(3)	Cl(1)–Zn(1)–Cl(2)	114.74(4)	Br(1)–Cd(1)–Br(2)	121.13(2)

Table 2 Four-coordinate geometry indices (τ_4) with representative examples from the literature

Complexes	Geometry	τ_4	THC_{DA}/100	FCGP/100	Ref.
Square planar (D_{4h})	Square planar	0.000	−1.43	−0.400	Yang *et al.*[51]
Trigonal pyramidal (C_{3v})	Trigonal pyramidal	0.850	0.000	1.00	Yang *et al.*[51]
[TEM(Co)Cl$_2$]	Tetrahedral	0.822	0.398	0.347	This work
[TEM(Zn)Cl$_2$]	Tetrahedral	0.891	0.407	0354	This work
[TEM(Cd)Br$_2$]	Tetrahedral	0.876	0.33	0.515	This work
[DE(Cd)Br$_2$][a]	Square planar	0.859	0.351	0.490	Nayab *et al.*[14]
[L$_B$(Zn)Cl$_2$][b]	Tetrahedral	0.862	0.388	0.397	Lee *et al.*[46]
[Lc(Co)Cl$_2$][c]	Tetrahedral	0.88	—	—	Kim *et al.*[56]
Tetrahedral (T_d)	Tetrahedral	1.00	1.00	0.000	Yang *et al.*[51]

[a] DE = (*E*)-N^1,N^1-diethyl-N^2-(thiophen-2-ylmethylene)-ethane-1,2-diamine. [b] L_B = 4-(quinolin-2-ylmethyl) morpholine. [c] L_C = (*E*)-N^1,N^1-dimethyl-N^2-(thiophen-2-ylmethylene)ethane-1,2-diamine.

pared with those in previously reported works and found to be distorted tetrahedral.[51,52] The N_{imine}–M–$N_{morpholine}$ bond angles for **[TEM(Co)Cl$_2$]** (85.90(8)°), **[TEM(Zn)Cl$_2$]** (85.76(14)°), and **[TEM(Cd)Br$_2$]** (79.32(10)°) are comparable with the corresponding parameter reported for the tetrahedral complexes.[52,53] The $Cl_{terminal}$–M–$Cl_{terminal}$ and $Br_{terminal}$–M–$Br_{terminal}$ bond angles in the studied complexes were found to be 112.52(3)°, 114.80(5)°, and 121.147(18)°, respectively. In addition, the angles between the five-membered *N*,*N*′-chelating ring and the thiophene ring in **[TEM(M)X$_2$]** are in the range of 17.55–21.82°, whereas those with the morpholine ring are 89.01–89.18°. The bond lengths of M–N_{imine} and M–$N_{morpholine}$ lie in the expected ranges of 2.035(2)–2.294(2) and 2.130(2)–2.347(6) Å, respectively. The M–$N_{morpholine}$ bond is longer than the M–N_{imine} bond probably because of the difference in the basicity and hybridization between the morpholine and the imine nitrogen atoms. These structural parameters agree well with those of the tetrahedral imine M(II) complexes.[54] As shown in Table 1, average M–Cl/Br and –N=C distances of 2.213(13)–2.530(6) and 1.280(3) − 1274(5) Å, respectively, are in the acceptable range.[54] The C(1)–C(2) bond distances in **[TEM(M)X$_2$]** (1.427(6) − 1.438(7) Å) fall in the acceptable range, reflecting delocalized π-electrons.[54]

The ligand topologies around the M(II) center were visualized and calculated using the SambVca 2.1 software.[55] The comparison of steric maps showed that **[TEM(Cd)Br$_2$]** has the least crowded environment with a V_{bur} value of 44.9%, whereas **[TEM(Co)Cl$_2$]** exhibits a V_{bur} value of 50.4%. The topographic steric maps of **[TEM(M)X$_2$]** presenting the steric bulk of the attached ligand around the M(II) centers are shown in Fig. 5.

3.3 Antimicrobial activities

3.3.1 Antileishmanial activity. Recently, complexes with sulfur-bearing moieties have been favored in the research on drugs against parasites causing leishmaniasis because of the similarity of these complexes to natural products with promising antileishmanial activities.[57] Herein, we also tested the prepared ligand and its M(II) complexes against the intracellular protozoa *L. major*. All tested compounds showed better antileishmanial activity than Amphotericin B (Table 3). The complex of Cd(II) shows good antileishmanial activity with IC_{50} value of 0.31 ± 0.01 μM and the ligand exhibits moderate activity with IC_{50} values of 0.74 ± 0.01 μM, as presented in Table 3. Thus, complexation enhances the activity of the ligand. The complexation of organic ligands with transition metals can enhance their activity. Among the studied compounds, antileishmanial inhibition at 50 μg mL^{-1} decreases in the following order: **[TEM(Cd)Br$_2$]** > **[TEM(Cu)Cl$_2$]** > **[TEM(Co)Cl$_2$]** > **[TEM(Zn)Cl$_2$]** > **TEM** (Table 3). The higher activity of the M(II) complexes than that of the free ligand was attributed to the improved lipophilicity of the complexes owing to chelation, based on Overtone's concept of cell permeability.[58–60] Notably,

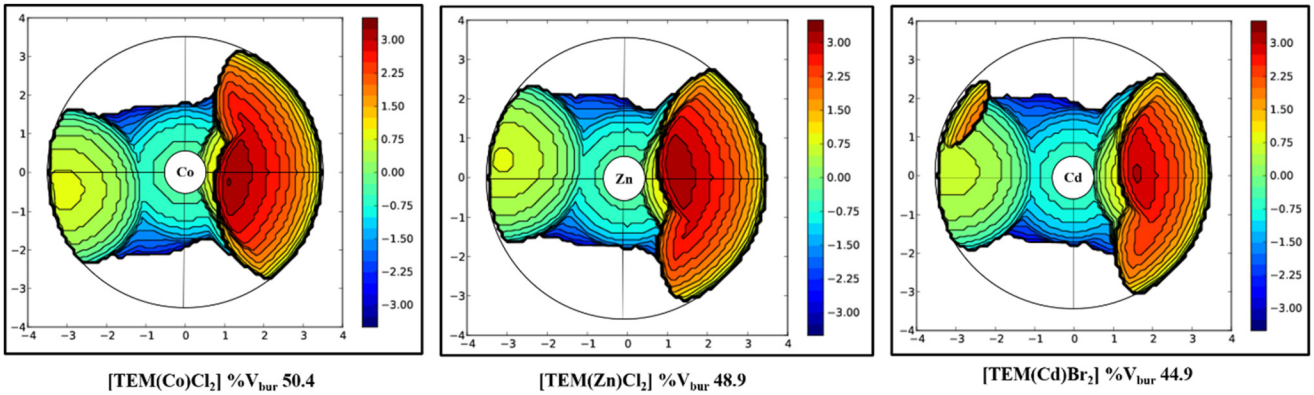

Fig. 5 Comparison of the topographic maps of **[TEM(M)X_2]** (M = Co and Zn; X = Cl; M = Cd, X = Br), complexes.

Table 3 Antileishmanial activity of **TEM** and its M(II) complexes against *L. major*

S. no	Samples	IC_{50} ± SEM[a] (μM)
1	**TEM**	0.74 ± 0.01
2	**[TEM(Co)Cl_2]**	0.39 ± 1.08
3	**[TEM(Cu)Cl_2]**	0.38 ± 0.00
4	**[TEM(Zn)Cl_2]**	0.42 ± 1.03
5	**[TEM(Cd)Br_2]**	0.31 ± 0.01
6	**(Amphotericin B)**	0.57 ± 1.06

[a] SEM = standard error mean (experiment run in triplicate).

these complexes could be adsorbed on the cell wall of microorganisms, disrupting cellular respiration and thus blocking the synthesis of proteins, which restricts the further growth of microorganisms. In addition, the mode of action involves the formation of hydrogen bonds between the active centers of various cellular constituents and azomethine and other donor groups, disturbing normal cellular processes.[60] The nature of the anion (Cl or Br) can also influence the activity of the metal complexes. Generally, complexes with bromide ligands tend to exhibit higher potential compared to their chloride analogues. This can be attributed to the greater polarizability, higher nucleophilic character and larger size of the bromide ligand, which can enhance the lipophilic character of the complex and facilitate its permeation through the lipid membrane of microbes.[61] Therefore, the antileishmanial activity of M(II) complexes cannot be ascribed solely to chelation; it seems to be an intricate blend of all the abovementioned contributions.[58–60]

3.3.2 Antioxidant activities. The overproduction of reactive oxygen species, including superoxide anions or radicals, facilitates the degradation of biomolecules, such as proteins, DNA, and lipids, playing a significant role in the inflammatory process induced by several human diseases.[62] Antioxidants can protect cells by decreasing oxidative stress that can cause damage to cells during metabolism. In this regard, transition metal complexes derived from Schiff base ligands are known for their antioxidant activity.[10,63] Thus, recently, the design of biomimicking models with additional biological applications has drawn the attention of bioinorganic chemists. The DPPH radical-scavenging method is an economic, accurate, and sensitive method for estimating the antioxidant potential of complexes. DPPH is a nitrogen-centered stable radical that can react with antioxidants, wherein it is reduced to nonradical species, which produces a change in absorption. The antioxidant activity of **TEM** and its M(II) complexes was screened *via* the DPPH free radical-scavenging assay. Antioxidant potential was estimated at different concentrations (10, 25, 50, 100, and 150 μg mL^{-1}) using ascorbic acid as a positive control. Notably, the antioxidant activity of the studied complexes increases with the concentration (Fig. S19†). The ligand shows moderate antioxidant activity, whereas metal complexes exhibit considerably higher antioxidant activities than the ligand. Specifically, **[TEM(Cd)Br_2]** exhibits the highest antioxidant activity, with an IC_{50} value of 6.01 ± 0.11 μM, whereas **[TEM(Co)Cl_2]** shows the lowest antioxidant activity, with an IC_{50} value of 17.22 ± 0.19 μM (Table 4). This trend in the antioxidant activities of the studied complexes can be explained by their structural properties. There is a possibility of the interference of **[TEM(Co)Cl_2]** with DPPH absorption at 517 nm, which might result in a slightly higher IC_{50} value compared to other metal complexes, as the Co(II) center can contribute to the absorption in this region. The antioxidant potential of the studied compounds decreases in the following order: **[TEM(Cd)Br_2]** > **[TEM(Cu)Cl_2]** > **[TEM(Zn)Cl_2]** > **[TEM(Co)Cl_2]** > **TEM** (Table 4). A comparative antioxidant assay of **[TEM(Cd)Br_2]** and **[TEM(Zn)Cl_2]** with identical ligand architecture and geometry (tetrahedral) revealed that the chloro-bearing complex

Table 4 Antioxidant activity of **TEM** and its corresponding M(II) complexes towards the scavenging of the DPPH radical compared to ascorbic acid

S. no	Compounds	IC_{50} ± SEM[a] (μM)
1	**TEM**	38.07 ± 0.28
2	**[TEM(Co)Cl_2]**	17.22 ± 0.19
3	**[TEM(Cu)Cl_2]**	11.98 ± 0.07
4	**[TEM(Zn)Cl_2]**	9.52 ± 0.22
5	**[TEM(Cd)Br_2]**	6.01 ± 0.11
6	**Ascorbic acid**	25.32 ± 1.02

[a] SEM = standard error mean (experiment run in triplicate).

showed lower potential as the chloride ions were attached firmly to the M(II) center, as evident from the bond lengths (Table 1). Furthermore, the Zn–Cl bond distance was smaller than the Cd–Br bond distance, thus restricting the approach of radicals to the M(II) center.[61] The buried volume also signifies the higher activity of **[TEM(Cd)Br$_2$]** than that of **[TEM(Zn)Cl$_2$]** owing to the different steric encumbrances experienced by these M(II) centers (Fig. 5).[64,65]

SAR was used to predict the relationship between structure and biological activity. All the synthesized complexes are remarkably active against the performed biological activities. The azomethine group (–HC═N–) and thiophene moiety present in these complexes are responsible for their biological responses. The synthesized Schiff base ligand, **TEM**, showed moderate antioxidant activity, but when the imine ligand was cyclised with Co(II), Cu(II), Zn(II), and Cd(II) metal ions, the potency of the compounds started increasing, which demonstrated that the metal framework was effective in oxidative stress management. The Cd(II) and Zn(II) complexes have the highest ability to control oxidation because of the metallic effect, binding affinity towards the cell, stable aromatic ring, lipophilicity, hydrophobicity, and DNA binding ability. This is evident from the previously reported complexes.[64,65] These complexes offer a promising avenue for the development of novel antioxidant agents with enhanced efficacy and specificity.

3.3.3. Urease inhibitory potential. Urease enzyme has been related to various gastrointestinal diseases, such as hepatic coma, encephalopathy, ulcers, and urinary catheter encrustation.[66] The urease activity can be decreased using inhibitors, which may constitute a promising remedy for peptic ulcers. Metal complexes inhibit the urease activity.[67] In particular, thiophene-based complexes possess strong anti-urease potential.[68,69] Herein, the studied complexes exhibit considerable urease inhibition activity (Table 5). Overall, **[TEM(Cd)Br$_2$]** demonstrated the greatest inhibitory effects against JB urease (IC_{50} = 4.51 ± 0.12 μM) and BP urease (IC_{50} = 3.50 ± 0.01 μM), notably higher than that of the standard thiourea (IC_{50} = 5.1 ± 0.05 and 4.10 ± 0.11 μM). **[TEM(Zn)Cl$_2$]** showed slightly low urease inhibitory effects against JB and BP ureases, with IC_{50} = 7.15 ± 1.11 and 8.05 ± 1.01 μM, respectively. The type of central metal ion, its coordination environment, and its coordination state affect the urease inhibitory profile of the complexes. For instance, Schiff base Cu(II) complexes of phenylethylamine derivatives have demonstrated strong urease inhibition; however, their Ni(II) counterparts have not, suggesting the important role of metal atoms in the inhibition of urease.[70] Herein, **TEM** exhibited much lower inhibitory activity than its M(II) complexes. Such a large difference in activity was attributed to the interactions of the metal center with the urease residues. Thus, the **[TEM(M)X$_2$]** complexes are used as antiulcer agents and hold great promise for formulating organometallic drugs. However, further investigations of the *in vivo* inhibitory potential of these complexes are required to understand their mode of action.

3.3.4. Evaluation of anticancer activity. One of the potential approaches towards the treatment of cancer is to design new metal complexes having labile sites and substituents. Many of these metal complexes initiate their activity *via* binding on the DNA molecule and result in the blocking of the division of cancer cells, resulting in cell death.[71] The *in vitro* cytotoxic potentials of the synthesized ligand and its M(II) complexes were screened against those of hepatic cancer HepG2, human colorectal cancer HCT-116, and breast cancer MCF-7 cell lines, and the results are presented in Table 6. The majority of the compounds are more active against the MCF-7 cell line than against the other cell lines. **TEM** and its respective M(II) complexes show high anticancer activities against HepG2, HCT-116, and MCF-7 cell lines, with IC_{50} values ranging from 2.2 ± 0.09 to 6.8 ± 0.11 μM. Notably, the central metal ion of the investigated complexes considerably affects the anticancer activity by varying the ability to bind to DNA. Evidently, the IC_{50} values of the studied complexes against MCF-7 and HCT-116 cancer cell lines are lower than those reported for 2-amino thiophene-derived M(III) complexes[72] but are similar to those of ethylenediamine-bis-acetylacetonate-derived M(II) complexes against the studied cancer cell lines.[73]

3.4. Molecular docking

The experimental results suggested the synthesized Schiff base metal complexes as a promising candidate for antileishmanial and anti-urease applications. To evaluate this, molecular

Table 5 Urease inhibition activities of **TEM** and its corresponding M(II) complexes

		IC_{50} ± SEM[a] (μM)	
Entry	Samples	JB urease	BP urease
1	**$CoCl_2·6H_2O$**	10.9 ± 0.13	12.9 ± 0.22
2	**$CuCl_2·2H_2O$**	12.2 ± 0.17	13.2 ± 0.17
3	**$ZnCl_2$**	15.2 ± 0.17	17.2 ± 0.17
4	**$CdBr_2·4H_2O$**	10.9 ± 0.01	11.9 ±1.11
5	**TEM**	17.4 ± 1.03	20.1 ± 1.05
6	**[TEM(Co)Cl$_2$]**	5.15 ± 1.09	6.25 ± 1.11
7	**[TEM(Cu)Cl$_2$]**	5.35 ± 0.10	6.51 ± 0.21
8	**[TEM(Zn)Cl$_2$]**	7.15 ± 1.11	8.05 ± 1.01
9	**[TEM(Cd)Br$_2$]**	4.51 ± 0.12	3.50 ± 0.01
10	**Thiourea**	5.1 ± 0.05	4.10 ± 0.11

[a] SEM = standard error mean (experiment run in triplicate).

Table 6 Cytotoxic activity of **TEM** and its M(II) complexes against HepG2, human colorectal cancer (HCT), and breast cancer MCF-7 cell lines

		IC_{50} ± SEM[a] (μM)		
Entry	Samples	HepG2	HCT-116	MCF-7
1	**TEM**	10 ± 0.04	11.1 ± 1.03	6.0 ± 1.00
2	**[TEM(Co)Cl$_2$]**	5.8 ± 1.11	5.0 ± 1.01	4.0 ± 1.06
3	**[TEM(Cu)Cl$_2$]**	6.8 ± 0.11	6.5 ± 0.21	5.9 ± 0.23
4	**[TEM(Zn)Cl$_2$]**	3.9 ± 0.07	3.6 ± 1.20	3.3 ± 0.01
5	**[TEM(Cd)Br$_2$]**	3.5 ± 0.30	2.7 ± 0.16	2.2 ± 0.09
6	**Vinblastine standard**	3.0 ± 0.05	2.8 ± 0.17	0.98 ± 0.22

[a] SEM = standard error mean (experiment run in triplicate).

docking was utilized to investigate the underlying mechanisms and physical interactions at the atomic and molecular levels.[74] Strains of *L. infantum* (2JK6) and *S. pasteurii* (2UBP) were selected. 2JK6 (residue chain A was selected), a crystal structure of *L. infantum*, which participates in thio-based metabolism, is considered a main target of therapeutic agents, which are used for treating leishmaniasis.[75,76] In the case of 2UBP (residue chain C was utilized), urease catalyzes the hydrolysis reaction, which could be a potential candidate for investigating structure-based design for a urease inhibitor.[77]

The 3D ligplots in Fig. 6 and 7 illustrate the molecular docking results, showing the interactions between selected receptors and **TEM** and its **[TEM(M)X_2]** complexes. To investigate the antileishmanial potential of the synthesized complexes, 2JK6 (*L. infantum*) was docked with the synthesized complexes (Fig. 6). The results revealed that **TEM** interacted

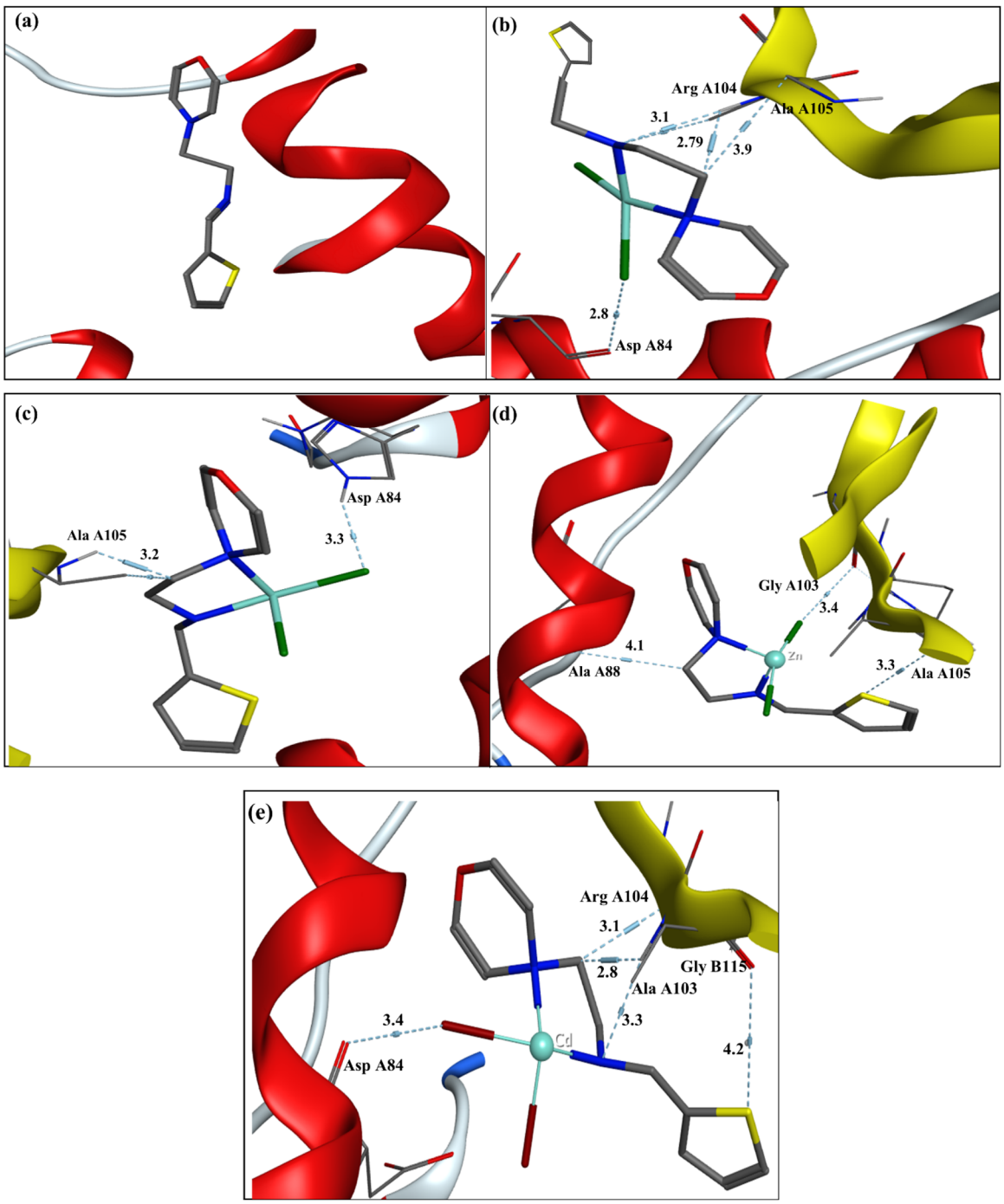

Fig. 6 3D ligplot illustrating molecular docked interaction of **TEM** and its metal complexes with the 2JK6 receptor alongside the corresponding lengths (Å) ((a): **TEM**, (b): **[TEM(Co)Cl_2]**, (c): **[TEM(Cu)Cl_2]**, (d): **[TEM(Zn)Cl_2]**, and (e): **[TEM(Cd)Br_2]**).

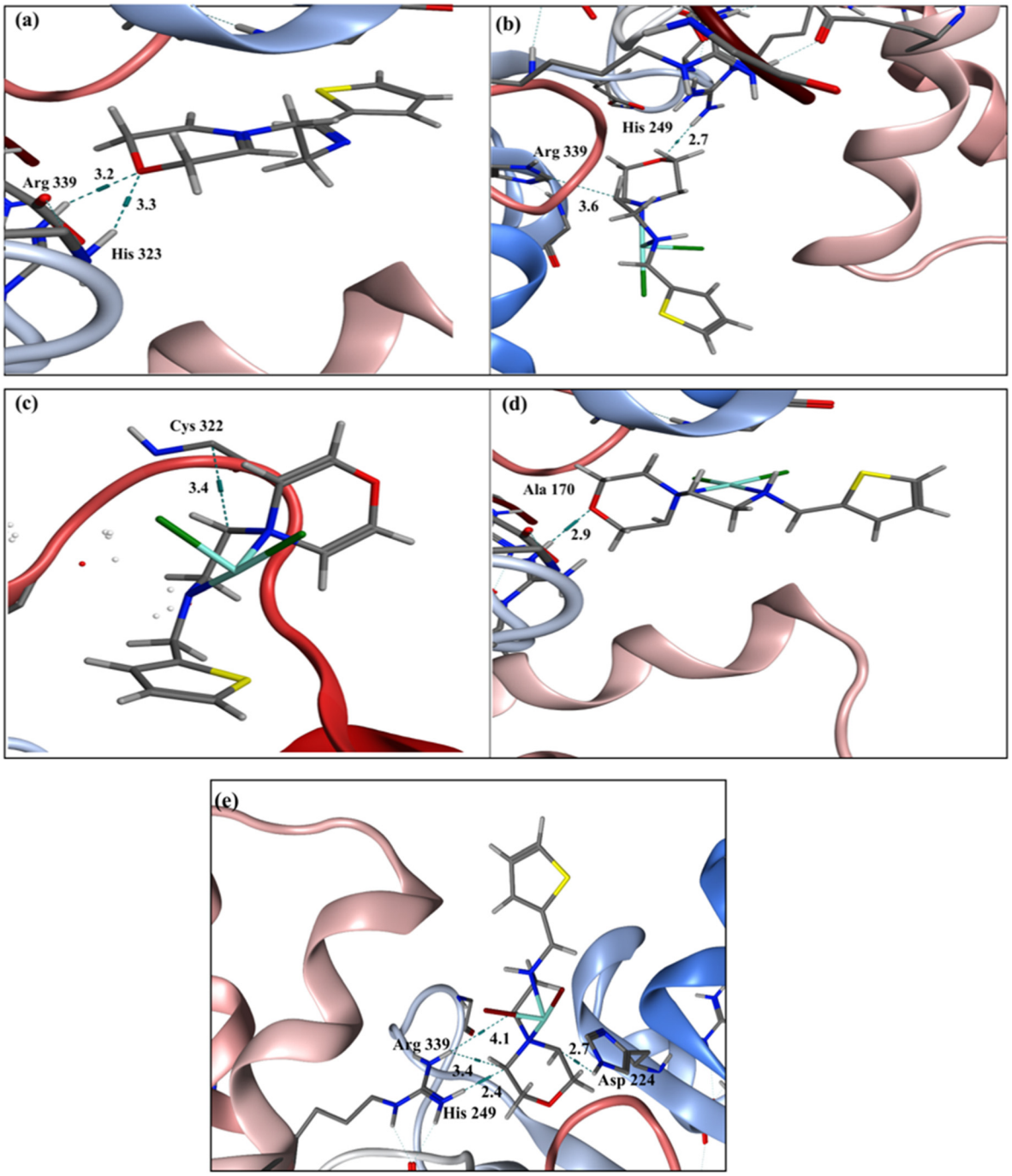

Fig. 7 3D ligplot illustrating molecular docked interaction of **TEM** and its metal complexes with the 2UBP receptor alongside the corresponding lengths (Å) ((a): **TEM**, (b): **[TEM(Co)Cl_2]**, (c): **[TEM(Cu)Cl_2]**, (d): **[TEM(Zn)Cl_2]**, and (e): **[TEM(Cd)Br_2]**).

with the Gly 56 residue through arene-hydrogen bonding. Furthermore, **[TEM(Co)Cl_2]** interacted with residue Cys 57, **[TEM(Cu)Cl_2]** with residues Leu A334 and Lys A60, and **[TEM(Zn)Cl_2]** with residues Thr 335 and Cys 57 through hydrogen bonding. Notably, **[TEM(Cd)Br_2]** showed a higher interaction capacity in the active pocket of 2JK6 through hydrogen bonding with Cys 52, Thr 335, and Cys 57, and arene-hydrogen bonding with Tyr 198.

In addition to the antileishmanial study, the synthesized metal complexes have the potential to interact to inhibit urease. **TEM** showed the interaction with the amino residue of Arg 339 and His 323 through hydrogen bonding, whereas **[TEM(Co)Cl_2]** interacted with the amino residue of 2UBP in an active pocket of the receptor protein, forming two hydrogen bonds with residues Arg 339 and His 249 by the formation of hydrogen bonds. Additionally, **[TEM(Cu)Cl_2]** engaged with the

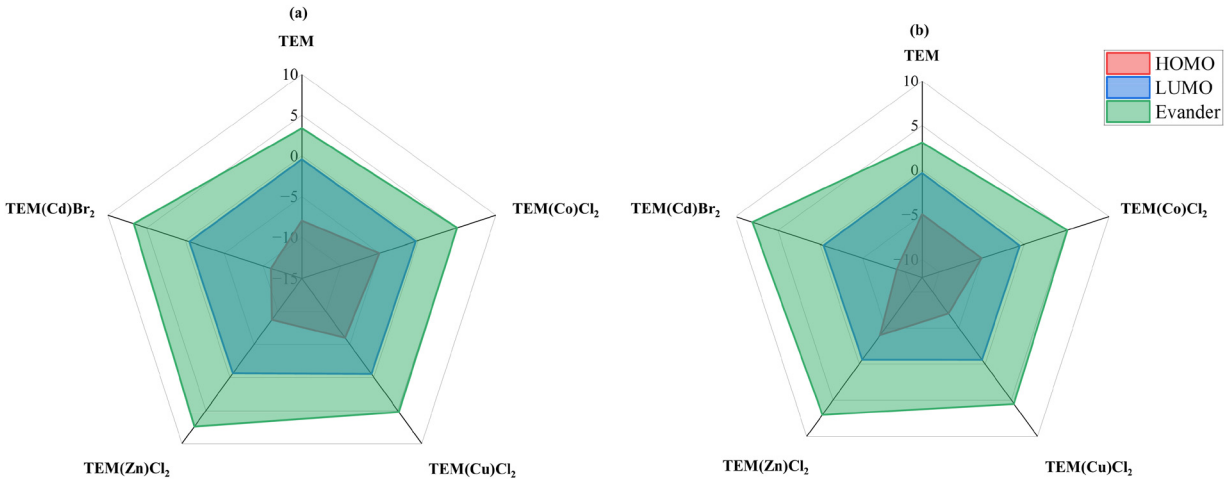

Fig. 8 Selected electronic descriptors obtained from molecular docking of (a) 2JK6 and (b) 2UBP.

active residues of Cys 322 by hydrogen bonding. In the case of **[TEM(Zn)Cl$_2$]**, only one hydrogen bond interaction occurred with Gln Ala 170 residues in the active pocket of the 2UBP receptor. Notably, **[TEM(Cd)Br$_2$]** exhibited interactions through four hydrogen bonds with Arg 339, His 249 and Asp 224. The **[TEM(Cd)Br$_2$]** inhibition potential aligned well with the experimental finding and showed exceptional activity. These results showed the dominant and pronounced participation of hydrogen bonding among other interactions. It is also anticipated that the **TEM** complexes exhibited a stronger interaction than the free ligand. The activity and interactions of **TEM** and its metal complexes with receptors were further evaluated by calculating the negative free energy, binding constant, steric and electronic descriptors, and surface electrostatic mapping. The calculated negative free energies are shown in Fig. S20,† indicating the spontaneous reactivity of all **TEM** metal complexes with receptors. The molecular docking results highlighted the higher antileishmanial and anti-urease potencies of the **TEM** complexes than those of the free ligand, *i.e.*, **TEM**. Notably, **[TEM(Cd)Br$_2$]** exhibits the lowest energy conformation and Gibbs energy across all cases, consistent with our experimental observations.

Alongside the Gibbs free energy, the binding constants were computed for **TEM** and its metal complexes with 2JK6 and 2UBP (Fig. S21†). **TEM** has a lower binding constant than the **TEM** complexes when subjected to docking. This underscores that the inhibition efficiency of these complexes greatly depends on their structural properties.[14] However, **[TEM(Cd)Br$_2$]** showed the highest bonding affinity in all cases.

Furthermore, the interaction between the selected strain and **TEM** ligands and their complexes was explored by calculating the physiochemical descriptors such as electronic and steric descriptors, and is shown in Fig. 8 and Table 7. The electronic descriptors, particularly the LUMO and HOMO, provided insights into the mechanism involved between strains and **TEM** and its metal complexes, based on the electron-donating and electron-accepting properties of the compound.

Table 7 Selected electronic descriptors obtained from molecular docking of 2JK6 and 2UBP with **TEM** and its corresponding M(II) complexes

	Electronic		Steric
	E_{ele} (kcal mol^{-1})	E_{total} (kcal mol^{-1})	H_f (kcal mol^{-1})
2JK6			
TEM	−305 193.0	−52 808.0	54.1
[TEM(Co)Cl$_2$]	—	—	19.0
[TEM(Cu)Cl$_2$]	—	—	19.0
[TEM(Zn)Cl$_2$]	−419 819.0	−68 140.0	20.0
[TEM(Cd)Br$_2$]	−411 655.0	−69 675.0	44.3
2UBP			
TEM	—	—	—
[TEM(Co)Cl$_2$]	—	—	54.2
[TEM(Cu)Cl$_2$]	53 242.1	−66 266.1	44.7
[TEM(Zn)Cl$_2$]	−42 561.3	−48 681.3	39.4
[TEM(Cd)Br$_2$]	−62 757.3	−68 523.9	70.8

In Fig. 8, the results indicate that the **TEM** complexes exhibit a lower HOMO and LUMO than **TEM**, demonstrating enhanced electron-accepting properties. The van der Waals force interactions and ionization potential energy also increased with the coordination of metals to the ligand. This observed trend suggests that the incorporation of transition metals facilitates interactions and enhances inhibition activity.

4. Conclusion

Herein, a novel Schiff base ligand, **TEM**, was synthesized in a good yield *via* a condensation reaction. The **TEM** complexes of Co(II), Cu(II), Zn(II), and Cd(II) were obtained by direct **TEM** ligation with metal salts. The structures of the synthesized ligand and its M(II) complexes were investigated using various spectroscopic techniques. The leishmanicidal and anti-oxidant activities of the synthesized ligand and its M(II) complexes were screened. **[TEM(Cd)Br$_2$]** showed prominent inhibitory potential, higher than the rest of the tested compounds under

identical experimental protocols. In the preliminary study, the investigated compounds showed considerable anticancer activity against human colorectal, hepatic, and breast cancer cell lines. These complexes also exhibited marked urease enzyme inhibition with IC_{50} values in the range of 3.50–8.05 μM. The relationship between their inhibitory activity and their structure was further demonstrated from the perspective of molecular docking. The results of molecular docking were consistent with the experimental results, confirming the highest antileishmanial and urease inhibition potential of **[TEM(Cd)Br_2]**. This study revealed various promising activities of the studied complexes, which may contribute to pharmacological assays and drug design.

Author contributions

Saira Nayab: supervision, conceptualization, methodology, analysis, and writing the original draft; Kalsoom Jan: molecular docking; Seung Hyeon Kim: supporting; Sa-Hyun Kim: supporting; Dilawar Farhan Shams: supporting; Younghu Son: supporting; Minyoung Yoon: X-ray diffraction studies; Hyosun Lee: writing – review editing-supporting.

Conflicts of interest

The authors declare that they have no known competing financial interests or personal relationships that could have appeared to influence the work reported in this paper.

Acknowledgements

This research was supported by the National Research Foundation of South Korea, funded by the Ministry of Education, Science, and Technology (MEST) (grant no. 2023R1A2C1005504). This work was also supported by the Technology Innovation Program (TIP # 20011123, Development of Cyclic Olefin Polymer [COP] with High Heat Resistance and High Transmittance) funded by the Korea Evaluation Institute of Industrial Technology (KEIT) and the Ministry of Trade, Industry and Energy (MOTIE, Republic of Korea). X-ray crystallography with the PLS-II 2D-SMC beamline was supported by MSIP and POSTECH.

References

1 A. M. S. Hossain, J. M. Méndez-Arriaga, C. Xia, J. Xie and S. Gómez-Ruiz, *Polyhedron*, 2022, **217**, 115692.
2 D. Iacopetta, J. Ceramella, A. Catalano, C. Saturnino, M. G. Bonomo, C. Franchini and M. S. Sinicropi, *Appl. Sci.*, 2021, **11**, 1877.
3 P. Ghanghas, A. Choudhary, D. Kumar and K. Poonia, *Inorg. Chem. Commun.*, 2021, **130**, e108710.
4 T. Vijayan, J. Kim, M. Azam, S. I. Al-Resayes, A. Stalin, B. S. Kannan, A. Jayamani, A. Ayyakannu and S. Nallathambi, *Appl. Organomet. Chem.*, 2022, e6542.
5 M. A. Malik, O. A. Dar, P. Gull, M. Y. Wani and A. A. Hashmi, *MedChemComm*, 2018, **9**, 409–436.
6 Y. Sun, Y. Lu, M. Bian, Z. Yang, X. Ma and W. Liu, *Eur. J. Med. Chem.*, 2021, **211**, 113098.
7 A. de Fátima, C. de P. Pereira, C. R. S. D. G. Olímpio, B. G. de F. Oliveira, L. L. Franco and P. H. C. da Silva, *J. Adv. Res.*, 2018, **13**, 113–126.
8 R. A. Ammar, A.-N. M. A. Alaghaz, M. E. Zayed and L. A. Al-Bedair, *J. Mol. Struct.*, 2017, **1141**, 368–381.
9 S. Chen, X. Liu, X. Ge, Q. Wang, Y. Xie, Y. Hao, Y. Zhang, L. Zhang, W. Shang and Z. Liu, *Inorg. Chem. Front.*, 2020, **7**, 91–100.
10 W. A. Zoubi, A. A. S. Al-Hamdani and M. Kaseem, *Appl. Organomet. Chem.*, 2016, **30**, 810–817.
11 S. N. Pandeya, D. Sriram, G. Nath and E. DeClercq, *Eur. J. Pharm. Sci.*, 1999, **9**, 25–31.
12 P. Krishnamoorthy, P. Sathyadevi, A. H. Cowley, R. R. Butorac and N. Dharmaraj, *Eur. J. Med. Chem.*, 2011, **46**, 3376–3387.
13 F. Arjmand, A. Jamsheera and D. K. Mohapatra, *J. Photochem. Photobiol.*, 2013, **121**, 75–85.
14 S. Nayab, A. Alam, N. Ahmad, S. W. Khan, W. Khan, D. F. Shams, M. I. Shah, M. Ateeq, S. K. Shah and H. Lee, *ACS Omega*, 2023, **8**, 17620–17633.
15 S. Yasmeen, S. H. Sumrra, M. S. Akram and Z. H. Chohan, *J. Enzyme Inhib. Med. Chem.*, 2017, **32**, 106–112.
16 R. Shah and P. K. Verma, *BMC Chem.*, 2019, **13**, 54.
17 Y. Ünver, S. Deniz, F. Çelik, Z. Akar, M. Küçük and K. Sancak, *J. Enzyme Inhib. Med. Chem.*, 2016, **31**, 89–95.
18 P. Panneerselvam, R. R. Nair, G. Vijayalakshmi, E. H. Subramanian and S. K. Sridhar, *Eur. J. Med. Chem.*, 2005, **40**, 225–229.
19 K. Ohui, E. Afanasenko, F. Bacher, R. L. X. Ting, A. Zafar, N. Blanco-Cabra, E. Torrents, O. Dömötör, N. V. May, D. Darvasiova, é. A. Enyedy, A. P.-B. J. Reynisson, P. Rapta, M. V. Babak, G. Pastorin and V. B. Arion, *J. Med. Chem.*, 2019, **62**, 512–530.
20 A. M. S. Hossain, J. M. M. Arriaga, C. Xia, J. Xie and S. G. Ruiz, *Polyhedron*, 2022, **217**, 115692.
21 A. B. Gündüzalp, İ. Özsen, H. Alyar, S. Alyar and N. Özbek, *J. Mol. Struct.*, 2016, **1120**, 259–266.
22 K. Sakthikumar, R. W. M. Krause and B. K. Isamura, *Bioinorg. Chem. Appl.*, 2022, 1–29, article ID 6987806.
23 R. M. D. da Cruz, F. J. B. Mendonça-Junior, N. B. de Mélo, L. Scotti, R. S. A. de Araújo, R. N. de Almeida and R. O. de Moura, *Pharmaceuticals*, 2021, **14**, 692.
24 L. Afroz, M. H. M. Khan, H. M. Vagdevi, M. Pari, R. M. Shafeeualla and K. M. M. Pasha, *Emergent Mater.*, 2022, **5**, 1133–1155.
25 A. A. El-Sherif and T. M. A. Eldebss, *Spectrochim. Acta, Part A*, 2011, **79**, 1803–1814.
26 A. Kumari and R. K. Singh, *Bioorg. Chem.*, 2020, **96**, 103578.

27 G. M. Sheldrick, *Acta Crystallogr., Sect. A: Found. Adv.*, 2015, **71**, 3–8.
28 S. Habtemariam, *BMC Pharmacol.*, 2003, **3**, 1–6.
29 I. P. Ejidike and P. A. Ajibade, *Bioinorg. Chem. Appl.*, 2015, **2015**, 890734.
30 M. W. Weatherburn, *Anal. Chem.*, 1967, **39**, 971–974.
31 M. Islam, A. Khan, M. T. Shehzad, A. Hameed, N. Ahmed, S. A. Halim, M. Khiat, M. U. Anwar, J. Hussain, R. Csuk, Z. Shafiq and A. Al-Harrasi, *Bioorg. Chem.*, 2019, **87**, 155.
32 L. H. Abdel-Rahman and A. M. A. Dief, *Appl. Organomet. Chem.*, 2019, **33**, e4943.
33 R. K. Al-Shemary, R. K. Mohapatra, M. Kumar, A. K. Sarangi, M. Azam, H. S. Tuli, A. Ansari, P. K. Mohapatra and K. Dhama, *J. Mol. Struct.*, 2023, **1275**, 134676.
34 N. S. Pagadala, K. Syed and J. Tuszynski, *Biophys. Rev.*, 2017, **9**, 91–102.
35 S. Nayab, S. Faisal, W. Khan, M. Ateeq, S. W. Khan, E. Kim and H. Lee, *Appl. Organomet. Chem.*, 2023, **37**, e7163.
36 A. A. Ajibola, F. Perveen, K. Jan, I. I. Anibijuwon, S. E. Shaibu, L. Sieroń and W. Maniukiewicz, *Crystals*, 2020, **10**, 991.
37 B. O. Aljohny, A. Rauf, Y. Anwar, S. Naz and A. Wadood, *ACS Omega*, 2021, **6**, 5878–5885.
38 A. S. Alturiqi, A.-N. M. A. Alaghaz, R. A. Ammar and M. E. Zayed, *J. Chem.*, 2018, **2018**, 1–17.
39 T. Seck, A. Sy, D. Lo, P. Gaye, M. Sall, O. Diouf, M. Diaw and M. Gaye, *Open J. Inorg. Chem.*, 2019, **9**, 35–52.
40 G. G. Mohamed, M. M. Omar and A. M. M. Hindy, *Spectrochim. Acta, Part A*, 2005, **62**, 1140–1150.
41 S. Park, J. K. Lee, H. Lee, S. Nayab and J. W. Shin, *Appl. Organomet. Chem.*, 2019, **33**, e4797.
42 Y. M. Rong, S. Yu and X. Yong-Jin, *SpringerPlus*, 2014, **3**, 701.
43 S. Kulandaivalu, Z. Zainal and Y. Sulaiman, *Int. J. Polym. Sci.*, 2016, **2016**, 1–12.
44 M. Vairalakshmi, R. Princess, B. K. Rani and S. J. Raja, *J. Chil. Chem. Soc.*, 2018, **63**, 1.
45 J. Lee, I. Melchakova, S. Nayab, K. Kim, Y. H. Ko, M. Yoon, P. Avramov and H. Lee, *ACS Omega*, 2023, **8**, 6016–6029.
46 J. Lee, K. Kim, H. Lee and S. Nayab, *Polyhedron*, 2021, **196**, 115003–115011.
47 K. Sultana, S. Zaib, N. U. H. Khan, I. Khan, K. Shahid, J. Simpson and J. Iqbal, *New J. Chem.*, 2016, **40**, 7084–7094.
48 H. E. Hashem, A. Nath and A. Kumer, *J. Mol. Struct.*, 2022, **1250**, 131915.
49 S. B. Kalia, K. Lumba, G. Kausal and M. Sharma, *Indian J. Chem.*, 2007, **46**, 1233–1239.
50 L. John, R. S. Joseyphus and I. H. Joe, *SN Appl. Sci.*, 2020, **2**, 500.
51 L. Yang, D. R. Powell and P. R. Houser, *Dalton Trans.*, 2007, 955–964.
52 K. Kim, S. Nayab, A. R. Jeong, Y. Cho, H. Yeo and H. Lee, *Inorg. Chim. Acta*, 2022, **539**, e121025.
53 S. Park, J. K. Lee, H. Lee, S. Nayab and J. W. Shin, *Appl. Organomet. Chem.*, 2019, **33**, e4797.
54 Y. Song, D. Kim, H.-J. Lee and H. Lee, *Bull. Korean Chem. Soc.*, 2014, **35**, 2929–2934.
55 L. Falivene, R. Credendino, A. Poater, A. Petta, L. Serra, R. Oliva, V. Scarano and L. Cavallo, *Organometallics*, 2016, **35**, 2286–2293.
56 K. Kim, S. Nayab, Y. Cho, H. Jung, H. Yeo, H. Lee and S.-H. Lee, *RSC Adv.*, 2022, **12**, 35896–35904.
57 F. Rodriguez, E. Iniguez, G. P. Contreras, H. Ahmed, T. E. M. M. Costa, R. Skouta and R. A. Maldonado, *Molecules*, 2018, **23**, 1626.
58 S. Ramakrishnan, E. Suresh, A. Riyasdeen, M. A. Akbarsha and M. Palaniandavar, *Dalton Trans.*, 2011, **40**, 3245–3256.
59 S. M. El-Megharbel, A. M. Adam, A. S. Meghdad and M. S. Refat, *Russ. J. Gen. Chem.*, 2015, **85**, 2366–2371.
60 H. E. Hashem, A. Nath and A. Kumer, *J. Mol. Struct.*, 2022, **1250**, 131915.
61 T. Chowdhury, S. Dasgupta, S. Khatua, K. Acharya and D. Das, *ACS Appl. Bio Mater.*, 2020, **3**, 4348.
62 F. Collin, *Int. J. Mol. Sci.*, 2019, **20**, 2407.
63 M. S. Alam and D.-U. Lee, *Bull. Korean Chem. Soc.*, 2015, **36**, 682–691.
64 B. Kumar, J. Devi, A. Dubey, A. Tufail and S. Sharma, *Inorg. Chem. Commun.*, 2024, **159**, 111674.
65 M. S. Aljahdali and A. A. El-Sherif, *Bioinorg. Chem. Appl.*, 2020, **2020**, 1–17, article ID 8866382.
66 F. Wang, L. Li, G. Zang, T. Deng and Z. You, *Acta Chim. Slov.*, 2020, **67**, 1155–1162.
67 M. Noreen, N. Rasool, Y. Gull, F.-ul.-H. Nasim, A. F. Zahoor, A. Yaqoob, S. Kousar, M. Zubair, I. H. Bukhari and U. A. Rana, *J. Saudi Chem. Soc.*, 2017, **21**, S403–S414.
68 S. Nayab, M. Khan, Y. Cho and H. Lee, *J. Coord. Chem.*, 2022, **75**, 2978–2999.
69 D. H. Shi, Z. L. You, C. Xu, Q. Zhang and H. L. Zhu, *Inorg. Chem. Commun.*, 2007, **10**, 404–406.
70 X. Dong, Y. Li, Z. Li, Y. Cui and H. Zhu, *J. Inorg. Biochem.*, 2012, **108**, 22–29.
71 T. Vijayan, M. Pugazhenthi, A. Nasirian, J. Kim, G. Kasi and A. Jayamani, *Bull. Korean Chem. Soc.*, 2022, **43**, 1284–1292.
72 M. Sumi, N. T. Nevaditha and B. S. Kumari, *J. Mol. Struct.*, 2023, **1272**, 134091.
73 A. Mijatović, N. Gligorijević, D. Ćoćić, S. Spasić, A. Lolić, S. Aranđelović, M. Nikolić and R. Baošić, *J. Inorg. Biochem.*, 2023, **244**, 112224.
74 R. R. Nasab, M. Mansourian and F. Hassanzadeh, *Res. Pharm. Sci.*, 2018, **13**, 509–522.
75 R. L. Krauth-Siege and M. A. Comini, *Biochim. Biophys. Acta, Gen. Subj.*, 2008, **1780**, 1236–1248.
76 C. Dumas, M. Ouellette, J. Tovar, M. L. Cunningham, A. H. Fairlamb, S. Tamar, M. Olivier and B. Papadopoulou, *EMBO J.*, 1997, **16**, 2590–2598.
77 S. Benini, W. R. Rypniewski, K. S. Wilson, S. Miletti, S. Ciurli and S. Mangani, *Structure*, 1999, **15**, 205–216.